

Chapter 4

Phase mixing damping of surface Alfvén wave in a slab plasma

4.1 Introduction

The first careful treatment of plasma wave in an inhomogeneous plasma was presented by Barston [39]. He applied the normal mode analysis to the electrostatic plasma waves in the inhomogeneous cold plasma for a plane-pinch. He considered two density profiles; one was everywhere continuous and nowhere constant, and the other was piecewise continuous and differentiable. It was shown that there exists no dispersion relation and the spectrum of frequency is continuous with real values in the former case. In the latter case discrete modes appear with the same number as that of discontinuities in the density profile. Sedláček [117] had studied the same problem using the Laplace transformation in time and showed that the normal mode approach is equivalent to the Laplace transformation approach. It was concluded that even in the continuous profile case, there exists a dispersion relation which Barston did not appreciate, and both continuous and discrete spectrum of frequency appear. The dispersion relation is interpreted in the same way as in the case of Landau damping in hot plasmas, and the discrete spectrum is considered as the ‘virtual’ eigenmode of the system.

Uberoi [141] has pointed out that there exists an interesting similarity of the forms between the equation governing Alfvén waves in the presence of an inhomogeneous magnetic field and that governing electrostatic plasma oscillations in a cold inhomogeneous plasma. By following Barston’s analysis, the incompressible Alfvén wave can be treated in the same way as the electrostatic plasma oscillation in the cold inhomogeneous plasma. Tataronis and Grossmann [75, 129] also followed Sedláček to study the incompressible shear Alfvén wave in the magnetized slab

plasma. While Tataronis and Grossmann assumed the incompressibility of plasma, Chen and Hasegawa [54] showed that the Alfvén wave damps in the inhomogeneous plasma without assuming incompressibility, and they proposed to use the Alfvén wave for heating the magnetically confined plasma [55].

Although these theories have mainly been developed for the surface waves at the plasma-vacuum interface, they will be applicable to an inhomogeneous plasma with a sharp density gradient formed by the injection of hydrogen ice pellet. Since the pellet is considered to be ablated in a narrow region, the density has a locally peaked profile. In the Heliotron-E experiment, magnetic fluctuations are often observed with the magnetic probe located near the wall of vacuum chamber [155], which are considered to be induced by the pellet injection. The frequency ω_r and damping rate ω_i are evaluated from experimental data as $\omega_r \sim 2.3 \times 10^6$ [s⁻¹] and $\omega_i \sim 6.9 \times 10^4$ [s⁻¹]. If we assume that this magnetic fluctuation is induced by Alfvén waves and that this damping is caused by plasma resistivity, the damping rate will be estimated as $10\text{-}10^2$ [s⁻¹]. Thus we need another mechanism to enhance the damping. The Alfvén resonance occurred in strongly inhomogeneous plasmas is such a candidate. It is noted that a detailed experimental investigation of Alfvén continuum damping is also reported in Ref. [51].

In Sec. 4.2, we show the wave equation for the shear Alfvén wave and discuss its general property. We derive the dispersion relation and analytic solution for the slab plasma with steep density gradient regions at the plasma surface in Sec. 4.4. In Sec. 4.6, we show the numerical solution of the dispersion relation. Our interest is in the dependence of damping rate on the scale length of density gradient. We present an interpretation that the pellet induced magnetic fluctuation disappears with a fairly large damping rate, when the singularity exists in the Alfvén wave equation at the surface of slab plasma.

4.2 Alfvén wave equation

Since we are interested in magnetic fluctuations in high density and high temperature plasmas, we use the ideal magnetohydrodynamic (MHD) equations for describing the wave phenomena. We consider a slab configuration with straight magnetic field lines for simplicity. It is a rough approximation for an annular high density plasma produced by the pellet injection into a toroidal plasma [155]. The equilibrium magnetic field is assumed in the z direction, and to vary only in the x direction; i.e.,

$$\mathbf{B}_0 = (0, 0, B_0(x)), \quad (4.1)$$

in the Cartesian coordinate. (In the toroidal plasma, x , y , and z correspond to radial, poloidal, and toroidal directions, respectively.) In addition, we assume that the equilibrium mass density ρ_0 and plasma pressure p_0 also vary only in the x direction.

The linearized ideal MHD equation is written as

$$\begin{aligned} \rho_0 \partial_t^2 \boldsymbol{\xi} = & -\nabla(\gamma p_0 \nabla \cdot \boldsymbol{\xi} + \boldsymbol{\xi} \cdot \nabla p_0) \\ & + \frac{1}{\mu_0} (\nabla \times \mathbf{B}_0) \times [\nabla \times (\boldsymbol{\xi} \times \mathbf{B}_0)] \\ & + \frac{1}{\mu_0} [\nabla \times (\nabla \times (\boldsymbol{\xi} \times \mathbf{B}_0))] \times \mathbf{B}_0, \end{aligned} \quad (4.2)$$

where $\boldsymbol{\xi}$, γ , and μ_0 denote the plasma displacement, the specific heat ratio, and permeability, respectively. We use the Fourier transformation in y and z , and the Laplace transformation in t ,

$$\tilde{\boldsymbol{\xi}}(x, k_\perp, k_\parallel, \omega) = \int_0^\infty dt \int_{-\infty}^\infty dy \int_{-\infty}^\infty dz \boldsymbol{\xi}(x, y, z, t) e^{i(\omega t - k_\perp y - k_\parallel z)}, \quad (4.3)$$

for $\boldsymbol{\xi}(x, y, z, t)$. By applying the Fourier-Laplace transformation to Eq. (4.2), the MHD wave equation is given as [54]

$$\frac{d}{dx} \left[\frac{\epsilon \alpha B^2}{\epsilon - \alpha k_\perp^2 B^2} \frac{d\tilde{\xi}_x}{dx} \right] + \epsilon \tilde{\xi}_x = S^*(x, k_\perp, k_\parallel, \omega), \quad (4.4)$$

where

$$\alpha(x) = 1 + \beta + \frac{\beta^2 k_\parallel^2 B^2}{\omega^2 \mu_0 \rho - \beta k_\parallel^2 B^2}, \quad (4.5)$$

$$\beta(x) = \frac{\gamma \mu_0 p}{B^2}, \quad (4.6)$$

$$\epsilon(x) = \omega^2 \mu_0 \rho - k_\parallel^2 B^2. \quad (4.7)$$

Here, the subscript zero which denotes equilibrium quantity is omitted, and $\tilde{\xi}_x$, and $S^*(x, \omega)$ denote the Fourier-Laplace transform of the x component of the plasma displacement vector, and the source term coming from initial conditions for the Laplace transform, respectively, and k_\parallel denotes the wavenumber parallel to equilibrium magnetic field (z direction), k_\perp the wavenumber in the y direction. The other components of the displacement vector $\tilde{\xi}_y$ and $\tilde{\xi}_z$ are expressed in terms of $\tilde{\xi}_x$ as,

$$\tilde{\xi}_y = -\frac{i\alpha k_\perp B^2}{\epsilon - \alpha k_\perp^2 B^2} \partial_x \tilde{\xi}, \quad (4.8)$$

$$\tilde{\xi}_z = \frac{-i\gamma \mu_0 p k_\parallel}{\omega^2 \mu_0 \rho - \beta k_\parallel^2 B^2} \frac{\epsilon}{\epsilon - \alpha k_\perp^2 B^2} \partial_x \tilde{\xi}. \quad (4.9)$$

The boundary conditions for Eq. (4.2) are given as $\tilde{\xi}_x \rightarrow 0$ in $x \rightarrow \pm\infty$, which correspond to the requirement that the normal component of the perturbed magnetic field vanishes at infinity. Notice that this MHD wave equation has a regular singularity at $\epsilon(x_0) = 0$ where the wave locally satisfies the dispersion relation of the homogeneous shear Alfvén wave. It is also noted that Eq. (4.4) is the slab simplified version of the Hain-Lust equation for the general screw pinch without magnetic shear.

To compare the above model with toroidal experiments, we assume that $|k_\perp|$, corresponding to poloidal wave number, is much larger than $|k_\parallel|$, corresponding to toroidal wave number, and $\beta \lesssim 1$. Since we consider the lower frequency wave than the ion cyclotron frequency, these conditions are equivalent to $|\alpha B^2 k_\perp^2| \gg |\epsilon|$, and therefore setting $S = -k_\perp^2 S^*$ leads to

$$\frac{d}{dx} \left[\epsilon(x, k_\parallel, \omega) \frac{d\tilde{\xi}_x}{dx} \right] - k_\perp^2 \epsilon(x, k_\parallel, \omega) \tilde{\xi}_x = S(x, k_\perp, k_\parallel, \omega). \quad (4.10)$$

It is noted that this equation also has a regular singularity at $\epsilon(x = x_0) = 0$.

Comparing Eq. (4.10) with the incompressible plasma model [129], we notice that the solution of Eq. (4.10) also describes an incompressible Alfvén wave. Though Eq. (4.4) contains both shear and compressional Alfvén wave, Eq. (4.10) only contains the shear Alfvén wave after $|k_\perp| \gg |k_\parallel|$ and $\beta \lesssim 1$ are assumed. This means that in large-aspect-ratio and low- β device, the shear Alfvén wave is prior to the compressional one.

4.3 Incompressible limit of spectral equation

In this section, we will discuss the consistency of the incompressibility condition by taking incompressible limit of the spectral ordinary differential equation (4.4).

Let us first show the relations among perturbed fields under the incompressible assumption. In the incompressible case [30, 110, 141], the slab Alfvén equation is written as

$$\left[\partial_t^2 - \frac{1}{\mu_0 \rho_0} (\mathbf{B}_0 \cdot \nabla)^2 \right] \boldsymbol{\xi}^{\text{ic}} = -\frac{1}{\rho_0} \nabla \left(p_1^{\text{ic}} + \frac{\mathbf{B}_0 \cdot \mathbf{B}_1^{\text{ic}}}{\mu_0} \right), \quad (4.11)$$

with the incompressibility condition

$$\nabla \cdot \boldsymbol{\xi}^{\text{ic}} = 0, \quad (4.12)$$

where the superscript ic denotes the perturbed fields under incompressible assumption. Here we will consider the same equilibrium magnetic field with the compressible

case (4.1). Hence, some tedious algebra gives the relation between y and z component of the displacement vector, perturbed pressure p_1^{ic} , and x component of the displacement vector in the Fourier transformed form as

$$\tilde{\xi}_y^{\text{ic}} = \frac{ik_{\perp}}{k_{\perp}^2 + k_{\parallel}^2} \partial_x \tilde{\xi}_x^{\text{ic}} \quad (4.13)$$

$$\tilde{\xi}_z^{\text{ic}} = \frac{ik_{\parallel}}{k_{\perp}^2 + k_{\parallel}^2} \partial_x \tilde{\xi}_x^{\text{ic}} \quad (4.14)$$

$$\tilde{p}_1^{\text{ic}} = \frac{\omega^2 \rho_0}{k_{\perp}^2 + k_{\parallel}^2} \partial_x \tilde{\xi}_x^{\text{ic}} - \tilde{\xi}_x^{\text{ic}} \frac{dp_0}{dx}, \quad (4.15)$$

where we have used the equilibrium relation

$$\frac{d}{dx} \left(p_0 + \frac{B_0^2}{2\mu_0} \right) = 0. \quad (4.16)$$

In order to take the incompressible limit of the physical quantities from the expression obtained under compressible condition, we can invoke the limit of $\gamma \rightarrow \infty$ as discussed in Appendix A. It is readily shown that the limit $\gamma \rightarrow \infty$ on the expressions (4.8) and (4.9) in the compressible case converges to the values (4.13) and (4.14) evaluated under incompressible condition, respectively. However, the expression of the pressure is not so trivial. Actually, simple substitution of Eqs. (4.13) and (4.14) into the adiabatic relation

$$\tilde{p}_1 = -\tilde{\xi} \cdot \nabla p_0 - \gamma p_0 (\nabla \cdot \tilde{\xi}) \quad (4.17)$$

will not give the same expression with Eq. (4.15). Since $\nabla \cdot \tilde{\xi}$ approaches to zero in the limit $\gamma \rightarrow \infty$, we have to include the higher order contributions in the second term of Eq. (4.17). Substituting the expressions (4.8) and (4.9) into Eq. (4.17), the perturbed pressure under compressible condition will be represented in terms of the x component of the displacement vector as

$$\begin{aligned} \tilde{p}_1 &= -\tilde{\xi}_x \frac{dp_0}{dx} - \gamma p_0 \partial_x \tilde{\xi}_x \left[1 + \frac{\alpha k_{\perp}^2 B^2}{\epsilon - \alpha k_{\perp}^2 B^2} + \frac{\gamma \mu_0 p k_{\parallel}^2}{\omega^2 \mu_0 \rho - \beta k_{\parallel}^2 B^2} \frac{\epsilon}{\epsilon - \alpha k_{\perp}^2 B^2} \right] \\ &= -\tilde{\xi}_x \frac{dp_0}{dx} - \frac{\gamma p_0 \epsilon \omega^2 \mu_0 \rho_0}{(\epsilon - \alpha k_{\perp}^2 B^2)(\omega^2 \mu_0 \rho_0 - \beta k_{\parallel}^2 B^2)} \partial_x \tilde{\xi}_x. \end{aligned} \quad (4.18)$$

By taking the limit $\gamma \rightarrow \infty$ directly on Eq. (4.18), it gives

$$\tilde{p}_1 \rightarrow -\tilde{\xi}_x \frac{dp_0}{dx} + \frac{\omega^2 \rho_0}{k_{\perp}^2 + k_{\parallel}^2} \partial_x \tilde{\xi}_x, \quad (4.19)$$

which exactly coincides with the relation (4.15) obtained with incompressible assumption.

Thus, it is conclude here that the incompressible result can be obtained by taking the limit $\gamma \rightarrow \infty$ on the relations from compressible system of equations, and this limit keeps exact consistency with the adiabatic equation of state.

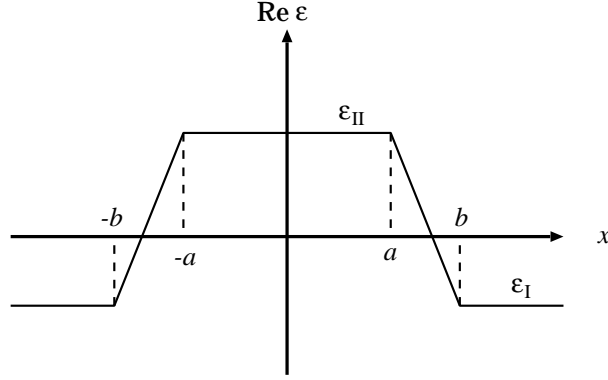


Figure 4.1: Profile of $\epsilon(x, k_{\parallel}, \omega) = \omega^2 \mu_0 \rho(x) - k_{\parallel}^2 B^2(x)$, where ϵ_I and ϵ_{II} are only functions of k_{\parallel} and ω . The positions $x = \pm b$ correspond to the surfaces of high density plasma.

4.4 Derivation of dispersion relation

Since the wave equation (4.10) is inhomogeneous, we can solve this equation by using a Green function. When the inverse Laplace transformation is carried out for $\tilde{\xi}$, the contribution from poles of the Green function becomes dominant for $t \rightarrow \infty$. For the magnetized plasma with sharp gradients near the surface regions, we assume a profile of ϵ which consists of three spatially constant regions and two linear ones described as

$$\epsilon(x, k_{\parallel}, \omega) = \begin{cases} \epsilon_I & (x < -b) \\ \delta x + \eta & (-b < x < -a) \\ \epsilon_{II} & (-a < x < a) \\ -\delta x + \eta & (a < x < b) \\ \epsilon_I & (b < x) \end{cases}, \quad (4.20)$$

where $\epsilon_I = \omega^2 \mu_0 \rho_I - k_{\parallel}^2 B_I^2$, $\epsilon_{II} = \omega^2 \mu_0 \rho_{II} - k_{\parallel}^2 B_{II}^2$, $\rho_{I,II}$ and $B_{I,II}$ are the constant values, and $\delta(k_{\parallel}, \omega) = (\epsilon_{II} - \epsilon_I)/(b - a)$, $\eta(k_{\parallel}, \omega) = (b\epsilon_{II} - a\epsilon_I)/(b - a)$. The schematic form which is symmetric with respect to x is illustrated in Fig. 4.1. This model may be applicable to an annular high density plasma produced by an injected ice pellet. The region $(-b, b)$ describes the high density one and the regions $(-\infty, -b)$ and (b, ∞) correspond to the background density ones. The following analysis to obtain the dispersion relation of shear Alfvén wave is parallel to that of Sedláček [117].

There exist non-collective oscillations due to the branch-point singularities of the Green function, which damp proportional to inverse power of time. Since the frequencies of these oscillations, however, depend on position, their behavior may not be seen from the outer magnetic probe [129]. Since the Green function also has simple poles in (a, b) and $(-b, -a)$, their contribution becomes dominant for $t \rightarrow \infty$.

Since Eq. (4.10) is an inhomogeneous differential equation of Sturm-Liouville type, the solution can be expressed in terms of the Green function, which can be written as

$$G(x, s; k_{\perp}, k_{\parallel}, \omega) = \begin{cases} J^{-1}[\tilde{\xi}_{(1)}(x, k_{\perp}, k_{\parallel}, \omega) \tilde{\xi}_{(2)}(s, k_{\perp}, k_{\parallel}, \omega)] & (x < s) \\ J^{-1}[\tilde{\xi}_{(1)}(s, k_{\perp}, k_{\parallel}, \omega) \tilde{\xi}_{(2)}(x, k_{\perp}, k_{\parallel}, \omega)] & (s < x) \end{cases}. \quad (4.21)$$

Here $\tilde{\xi}_{(1)}$ and $\tilde{\xi}_{(2)}$ are homogeneous solutions of the differential equation (4.10) with satisfying the boundary condition at $x = -\infty$ and $x = \infty$, respectively, J is the conjunct of $\tilde{\xi}_{(1)}$ and $\tilde{\xi}_{(2)}$,

$$\begin{aligned} J(k_{\perp}, k_{\parallel}, \omega) &= \epsilon(x) \left[\tilde{\xi}_{(1)} \frac{d\tilde{\xi}_{(2)}}{dx} - \frac{d\tilde{\xi}_{(1)}}{dx} \tilde{\xi}_{(2)} \right] \\ &= \frac{1}{2} k_{\perp} \epsilon_{\parallel} z_1 z_4 e^{2k_{\perp} a} D(k_{\perp}, k_{\parallel}, \omega), \end{aligned} \quad (4.22)$$

which can be proved independent of x and s . Here we have introduced the dispersion function

$$\begin{aligned} D(k_{\perp}, k_{\parallel}, \omega) &= ([I_0(z_2) + I_1(z_2)][K_0(z_1) + K_1(z_1)] - [I_0(z_1) - I_1(z_1)][K_0(z_2) - K_1(z_2)]) \\ &\quad \times ([I_0(z_3) - I_1(z_3)][K_0(z_4) - K_1(z_4)] - [I_0(z_4) + I_1(z_4)][K_0(z_3) + K_1(z_3)]) \\ &\quad + e^{-4k_{\perp} a} ([I_0(z_2) - I_1(z_2)][K_0(z_1) + K_1(z_1)] - [I_0(z_1) - I_1(z_1)][K_0(z_2) + K_1(z_2)]) \\ &\quad \times ([I_0(z_4) + I_1(z_4)][K_0(z_3) - K_1(z_3)] - [I_0(z_3) + I_1(z_3)][K_0(z_4) - K_1(z_4)]), \end{aligned} \quad (4.23)$$

and z_i ($i = 1-4$) which depend on k_{\perp} , k_{\parallel} , and ω denote the quantity associated with the scale length of the density gradient,

$$z_1 = -z_4 = \frac{\epsilon_{\parallel}}{\epsilon_{\parallel} - \epsilon_{\perp}} k_{\perp} (b - a), \quad (4.24)$$

$$z_2 = -z_3 = \frac{\epsilon_{\parallel}}{\epsilon_{\parallel} - \epsilon_{\perp}} k_{\perp} (b - a), \quad (4.25)$$

and I_n and K_n denote the n -th order modified Bessel function of the first and the second kind, respectively.

With the Green function (4.21), the solution for Eq. (4.10) is described as

$$\tilde{\xi}_x(x, k_{\perp}, k_{\parallel}, \omega) = \int_{-\infty}^{\infty} G(x, s; k_{\perp}, k_{\parallel}, \omega) S(s, k_{\perp}, k_{\parallel}, \omega) ds. \quad (4.26)$$

Then the plasma displacement in the real space is expressed by carrying out the inverse Fourier-Laplace transformation of Eq. (4.26),

$$\boldsymbol{\xi}(x, y, z, t) = \frac{1}{(2\pi)^3} \int_{\mathcal{C}} d\omega \int_{-\infty}^{\infty} dk_{\perp} \int_{-\infty}^{\infty} dk_{\parallel} \tilde{\boldsymbol{\xi}}(x, k_{\perp}, k_{\parallel}, \omega) e^{i(k_{\perp} y + k_{\parallel} z - \omega t)}, \quad (4.27)$$

where \mathcal{C} denotes the integration path in the complex ω plane. When there exist poles of the Green function, their contribution becomes dominant in the limit $t \rightarrow \infty$. Therefore $J = 0$ gives a dispersion relation:

$$D(k_{\perp}, k_{\parallel}, \omega) = 0. \quad (4.28)$$

Although the discussion of this paper is mainly concerned with density gradient, dispersion relation (4.28) is applicable to the case with inhomogeneous magnetic field.

4.5 Analytic solutions of dispersion relation

If we assume that the density gradients are steep, $|k_{\perp}(b-a)| \ll 1$, to obtain the analytic solution, the dispersion relation (4.28) has two branches shown as

$$\coth(k_{\perp}a) + \frac{z_2}{z_1} + z_2 \log \frac{z_2}{z_1} = 0, \quad (4.29)$$

$$\tanh(k_{\perp}a) + \frac{z_2}{z_1} + z_2 \log \frac{z_2}{z_1} = 0. \quad (4.30)$$

We need to consider Riemannian sheets for the logarithmic function with complex argument. Since there exist no solution on $n = 0$ Riemannian sheet, we carry out the analytic continuation into the other sheets and then calculate the weakest damping solution (or $|\omega_r| \gg |\omega_i|$ in $\omega = \omega_r + i\omega_i$). Two solutions exist on the $n = 1$ sheet, which are expressed as

$$\left\{ \begin{array}{l} \omega_{r1} = k_{\parallel} \sqrt{\frac{B_I^2 + \theta B_{II}^2}{\mu_0(\rho_I + \theta\rho_{II})}}, \\ \frac{\omega_{i1}}{\omega_{r1}} = -\frac{1}{4}\pi\theta k_{\perp}(b-a)(1 - e^{-2k_{\perp}a}) \\ \quad \times \frac{\mu_0\rho_I\rho_{II}(V_{AI}^2 - V_{AII}^2)}{(\rho_I + \theta\rho_{II})(B_I^2 + \theta B_{II}^2)}, \end{array} \right. \quad (4.31)$$

$$\left\{ \begin{array}{l} \omega_{r2} = k_{\parallel} \sqrt{\frac{\theta B_I^2 + B_{II}^2}{\mu_0(\theta\rho_I + \rho_{II})}}, \\ \frac{\omega_{i2}}{\omega_{r2}} = -\frac{1}{4}\pi k_{\perp}(b-a)(1 - e^{-2k_{\perp}a}) \\ \quad \times \frac{\mu_0\rho_I\rho_{II}(V_{AI}^2 - V_{AII}^2)}{(\theta\rho_I + \rho_{II})(\theta B_I^2 + B_{II}^2)}, \end{array} \right. \quad (4.32)$$

respectively, which describe the surface Alfvén waves. Here $\theta = \tanh(k_{\perp}a)$ is the parameter associated with the width of central constant density region, and V_A denotes the Alfvén velocity. Subscripts I and II denote the central and outer constant

regions in Fig. 4.1, respectively. It can be easily shown that the solutions on the other Riemannian sheets damp faster than those on the $n = 1$ sheet by replacing π in ω_{i1} and ω_{i2} with $(2n - 1)\pi$.

Both real frequencies ω_{r1} and ω_{r2} are proportional to k_{\parallel} , which is the same as the frequency of shear Alfvén wave in homogeneous plasmas, however, they include the parameter θ dependent on k_{\perp} . The damping rates are proportional to the scale length of the density gradient, $b - a$, and $|\omega_{i1}|$ and $|\omega_{i2}|$ are nearly equal to each other. Therefore, in the sharp boundary limit ($b - a \rightarrow 0$), these modes show undamped oscillations. When the distance of two density gradient regions, $2a$, goes to infinity with keeping $(b - a)$ constant, both the frequencies and damping rates of these two branches converge to the same value, which coincides with Chen and Hasegawa [54].

4.6 Numerical solutions of dispersion relation

In order to evaluate accuracy of the analytic solutions in Eqs. (4.31) and (4.32), numerical solutions of Eq. (4.28) are shown for the particular parameters. In the numerical calculations, it is useful to define the following dimensionless variables:

$$\begin{aligned} \hat{b} &= \frac{b}{a}, & \hat{\rho} &= \frac{\rho_{\text{II}}}{\rho_1}, & \hat{k}_{\parallel} &= k_{\parallel}a, & \hat{k}_{\perp} &= k_{\perp}a, \\ \hat{\omega}^2 &= \frac{\omega^2 a^2}{B_1^2 / \mu_0 \rho_1}, & \hat{\beta} &= 1 - \left(\frac{B_{\text{II}}}{B_1}\right)^2. \end{aligned} \quad (4.33)$$

Then the arguments of the modified Bessel functions are expressed in terms of these variables as

$$z_1 = \hat{k}_{\perp}(\hat{b} - 1) \frac{\hat{\omega}^2 - \hat{k}_{\parallel}^2}{\hat{\omega}^2(\hat{\rho} - 1) + \hat{k}_{\parallel}^2 \hat{\beta}}, \quad (4.34)$$

$$z_2 = \hat{k}_{\perp}(\hat{b} - 1) \frac{\hat{\omega}^2 \hat{\rho} - \hat{k}_{\parallel}^2(1 - \hat{\beta})}{\hat{\omega}^2(\hat{\rho} - 1) + \hat{k}_{\parallel}^2 \hat{\beta}}. \quad (4.35)$$

The numerical solutions of the dispersion relation (4.28) corresponding to ω_1 and ω_2 are shown in Fig. 4.2. Here we have used the following values for dimensionless parameters,

$$\hat{k}_{\perp} = 1, \quad \hat{k}_{\parallel} = 0.01, \quad \hat{\beta} = 0, \quad \hat{\rho} = 6, \quad (4.36)$$

and we have taken into account of the $n = 1$ Riemannian sheet. Though the damping rates are proportional to the scale length of the density gradient in the sharp boundary limit, they do not continue to increase monotonically with the scale length. They have extrema at $\hat{b} \simeq 1.9$ for ω_1 and $\hat{b} \simeq 1.4$ for ω_2 , and when the scale length of the density gradient becomes larger than this value, they turn out

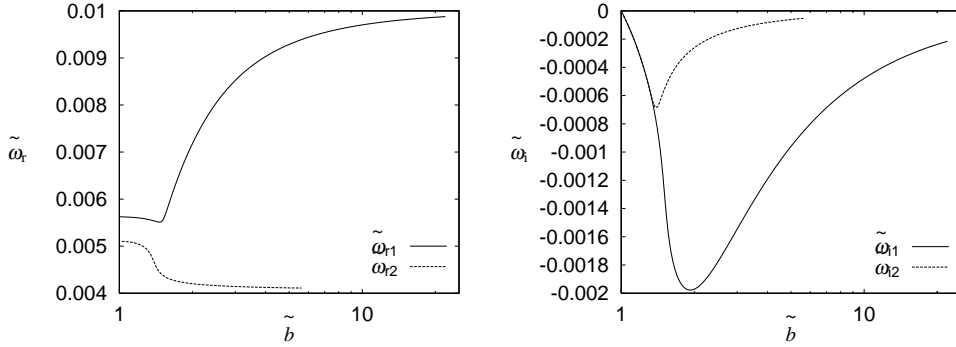


Figure 4.2: Dependence of normalized frequency $\hat{\omega}_r$ and damping rate $\hat{\omega}_i$ on the scale length of the density gradient. The left figure denotes the frequency and the right one the damping rate. The subscripts 1 and 2 denote the solutions of the exact dispersion relation (4.28) corresponding to Eq. (4.31) and (4.32), respectively.

to decrease with increase of \hat{b} . It is considered that $\hat{\omega}_i$ finally go to zero in the limit $\hat{b} \rightarrow \infty$. Also, $\hat{\omega}_{r1}$ is considered to have a limiting value of 0.01, which is equivalent to the relation $\omega = k_{\parallel} V_{A\text{I}}$. On the other hand, $\hat{\omega}_{r2}$ is considered to have a limiting value of $0.01 \times \sqrt{1/6}$, which is equivalent to the relation $\omega = k_{\parallel} V_{A\text{II}}$. In the region with $\hat{b} \sim 1$, we observe that the analytic solutions (4.31) and (4.32) agree with numerical results. In this region these two branches have almost the same damping rates, however, in the region $\hat{b} \gtrsim 1.5$, the branch ω_2 , which has a smaller frequency, has weaker damping rate than ω_1 . Since the density profile approaches to a homogeneous one at $\rho = \rho_1$ with increase of the scale length of the density gradients, $b - a$, the branch ω_2 remains prior to the other. We also observed that the maximum points of the damping rates go to the right with the increase of the fraction of the density $\hat{\rho}$. They do not move leftward or rightward due to the change of $\hat{\beta}$, although the damping rates themselves increase.

Figure 4.3 shows the deviation of the analytic damping rate from the numerical one. Here the same parameters as in Eq. (4.36) are used. The analytic solution is valid only for the case with the steep density gradient $\hat{b} \lesssim 1.2$. The error of the analytic solution is about 10% at $\hat{b} = 1.2$.

4.7 Summary

It is confirmed that two branches of the surface Alfvén wave exist for the slab plasma, since there are two sharp jump regions of density. However, the frequencies and damping rates of both branches are almost comparable, when the density jump is substantial. It is interpreted that the magnetic fluctuations induced by the pellet

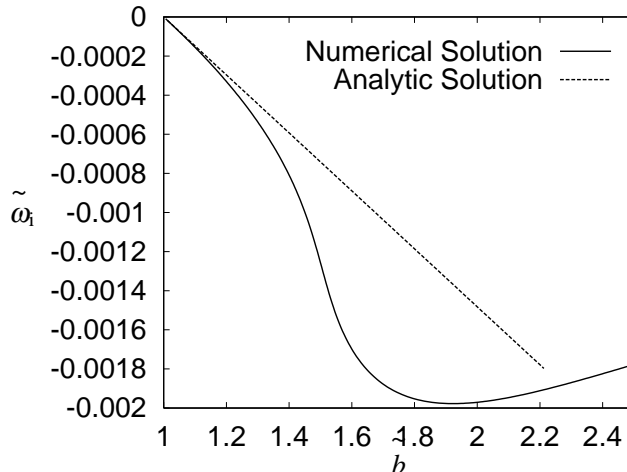


Figure 4.3: Comparison between analytic solution and numerical one of damping rate $\hat{\omega}_{i1}$ in Fig. 4.2. The normalized frequency of the analytic solution $\hat{\omega}_{r1}$ is independent of the scale length of the density gradient.

injection in Heliotron-E are surface Alfvén waves corresponding to Eq. (4.31) or Eq. (4.32). These modes damp with finite scale length of the density gradient. In the limit of sharp boundary, $(b - a) \rightarrow 0$, Eqs. (4.31) and (4.32) give undamped oscillations, and so do in the limit of homogeneous plasma, $(b - a) \rightarrow \infty$. That is to say, these two modes exist in the sharp boundary limit, while continuous spectrum does not appear.

The initial annular density profile produced by the pellet may have sharp density gradients satisfying $\hat{b} \gtrsim 1$, and the analytic treatment is valid to estimate ω_r and ω_i for comparison with experiments. For example, provided typical plasma parameters for Heliotron-E are assumed as $B_I = B_{II} = 1.9$ [T], $n_I = 10^{19}$ [m⁻³], $n_{II} = 6n_I$, $a = 10^{-1}$ [m], $b - a = 10^{-2}$ [m], $k_{\perp} = 10$ [m⁻¹], and $k_{\parallel} = 2 \times 10^{-2}$ [m⁻¹], we obtain $\omega_{r1} \sim 2 \times 10^6$ [s⁻¹], and $\omega_{i1} \sim 6 \times 10^4$ [s⁻¹], which is comparable to the experimental values expressed in the introduction, and the frequency ω_{r1} is much less than the ion cyclotron frequency $\omega_{ci} \sim 1.8 \times 10^8$. The damping rate is enhanced with the decrease of the density gradient by radial particle transport.